行政院國家科學委員會專題研究計畫　成果報告

輸電塔群於不同幾何排列下之非線性震力分析

計畫類別：個別型計畫
計畫編號：NSC93-2211-E-032-008-
執行期間：93 年 08 月 01 日至 94 年 07 月 31 日
執行單位：淡江大學土木工程學系

計畫主持人：雷英暉

計畫參與人員：簡育琳　蔡佳宏

報告類型：精簡報告

處理方式：本計畫可公開查詢

中　華　民　國 94 年 9 月 21 日

行政院國家科學委員會專題研究計畫成果報告

輸電塔群於不同幾何排列下之非線性震力分析

Nonlinear Seismic Analysis of Transmission Towers Under Various Line Configurations

計畫編號：NSC-93-2211-E-032-008

執行期限：93 年 8 月 1 日至 94 年 7 月 31 日

主持人：雷英暉　　淡江大學土木工程學系

計畫參與人員：簡育琳 蔡佳宏　　淡江大學土木工程學系

1. Abstract

In this paper, the dynamic behavior of a group of transmission towers linked together through electrical wires and subjected to a strong ground motion will be investigated in detail. In performing the seismic analysis, the wires and the towers concerned are modeled, respectively, by using the efficient cable elements and the 3-D beam elements both considering geometric nonlinearities. In addition, to enhance the reliability and applicability of analytical outcome, a sophisticated soil-structure interaction model will be utilized in analyses. The strength capacities and the fracture occurrences for the main members of the transmission tower are examined with the employment of the appropriate strength interaction equations. It is expected that by aid of this investigation, those who are engaged in code constitution or in practical designing of transmission towers may gain a better insight into the roles played by the interaction force between towers and wires and by the configurations of transmission lines under strong earthquake.

Keywords: *Chi-Chi earthquake, geometric nonlinearity, soil-structure interaction.*

中文摘要

發電廠於傳輸電力至不同住宅或工商業區之過程中，相關傳輸路線常因配合地形及地貌而呈俯仰轉折之多變走勢；影響所及，各個輸電塔將因承受來自不同水平及垂直方向之電纜拉力而產生不同之受震行為。本文除擬採用空間樑-柱元素來模擬各輸電塔之塔體結構外，並擬採用有效之纜索元素來模擬懸垂於相鄰輸電塔間之高壓電纜，期能徹底瞭解整體塔群系統在不同地質地貌下，其各別桿件變形及受力之差異性；為使分析結果更具可靠性及實用性，構件之幾何與材料非線性行為應予考慮，並將精密之土壤-結構互制模式及構件破壞指數予以採用。研究結果顯示，於強震作用下，塔群之行徑路線確將對輸電塔群之受力及非線性行為造成明顯之影響。

關鍵詞：*集集地震，幾何非線性，土壤結構互制*

2. Introduction

The importance of the transmission tower on national economy and people's living has been well recognized. During the attack of the Chi-Chi earthquake, with a size of 7.3 in Ritcher magnitude, in Taiwan on Sept. 21, 1999, over two thousand four hundred residents were killed. Besides, the strong vibration of the ground motion has caused the collapse of a pivotal transmission tower located in the central region of the state. As a result, the government was forced to take measures of reducing electricity supply for more than six weeks. During this period, a great inconvenience of living was brought to the people, and a huge commercial loss was incurred in the high-tech industry of the island

To achieve the aim of supplying electricity everywhere in a country, many transmission towers are hence built in the rugged circumstances of climbing mountains or crossing rivers. Accordingly, the elevation at which some tower structures are located may differ from that associated with other transmission towers. Moreover, the marching route of the tower procession in such circumstances may

exhibit in an extremely irregular manner. This variation on either the elevation or the orientation for the geometric configuration of a group of transmission towers would certainly affect the interaction force between electrical wires and tower structures.

The conventional seismic analysis of transmission towers is usually undertaken by taking each of towers as an isolated structure without taking the inertia coupling and the strong traction of high-voltage cables lining up in various directions into account. Furthermore, many of structural engineers were used to simply ignore all wire masses or to take them as the lumped ones affiliated to the tower in seismic analysis. The results obtained by following such analytical schemes would not be able to reflect the actual forced conditions of the tower structure itself as well as the base foundation beneath it.

Being slender and tall in appearance, the transmission tower is destined to be susceptible to the effect of geometric nonlinearity. In addition, either the cable mass of structural system in which transmission towers are spaced over a long distance or the soil-structure interaction, especially for the cases where tower structures are built on the soft ground, would be expected to bring noticeable influences on the dynamic behavior of the structure. In this paper, the cable element proposed by Desai *et al.* and verified efficient in dynamic cable analysis will be used for the modeling of electrical wires[1]. In formulation of beam-column elements employed for modeling the tower members, the effect of geometric nonlinearity will be considered. Furthermore, the influence of soil-structure interaction on the seismic responses of transmission towers will be considered by incorporating a sophisticated interaction model proposed by Wolf and Song [2-4] into the global tower system.

2. Formulation of structural modeling

All seismic analyses in this paper are undertaken with respect to the structural system composed of various portions including electrical wires, tower structures, near-field soil blocks and end-restraint springs, as indicated in Fig. 1. The formulation involved in the modeling of each portion of the system will be presented in the following.

2.1 Electrical wires and end-restraint springs

Being highly flexible and undergoing significant deformations, the electrical wire should therefore be analyzed in the manner of taking the effect of geometric nonlinearity into account. The formulation for the 3-node, iso-parametric cable element proposed by Desai, Popplewell and Shah for describing the dynamic behavior of transmission lines is presented in the following [1].

Consider the cable element referred to the fixed global X, Y, Z coordinates and the initial intrinsic coordinate S, in the manner illustrated in Fig. 2.

As an iso-parametric finite element, the global coordinates and displacements at any point of the cable element considered will be given, respectively, by

$$\begin{bmatrix} X & Y & Z \end{bmatrix}^T = \sum_{K=1}^{3} N_K \begin{bmatrix} X_K & Y_K & Z_K \end{bmatrix}^T \tag{1}$$

In Eq.(1), X_K, Y_K, Z_K are the global nodal coordinates corresponding to node K, and the parabolic shape functions, N_K, are

$$N_1 = \frac{2S^2}{L_c^2} - \frac{3S}{L_c} + 1 \tag{2}$$

$$N_2 = -\frac{4S^2}{L_c^2} - \frac{4S}{L_c} \tag{3}$$

$$N_3 = \frac{2S^2}{L_c^2} - \frac{S}{L_c} \tag{4}$$

Following the standard finite element procedure, one can obtain the elemental consistent mass matrix in terms of the relation given by

$$\begin{bmatrix} \boldsymbol{M}^e \end{bmatrix} = \int_0^{L_c} [\boldsymbol{N}]^T [\boldsymbol{\mu}][\boldsymbol{N}] dS \tag{5}$$

To account for the geometric deformations of the cable, the elemental stiffness matrix $\begin{bmatrix} \boldsymbol{K}_T^e \end{bmatrix}$ is decomposed into

$$\begin{bmatrix} \boldsymbol{K}_T^e \end{bmatrix} = \begin{bmatrix} \boldsymbol{K}^e \end{bmatrix} + \begin{bmatrix} \boldsymbol{K}_\sigma^e \end{bmatrix} \tag{6}$$

In formulation of $\begin{bmatrix} \boldsymbol{K}^e \end{bmatrix}$, the elemental strain vector $\{\boldsymbol{\varepsilon}\}$ and stress vector $\{\boldsymbol{\sigma}\}$ are

expressed, respectively, in the form of

$$\{\boldsymbol{\varepsilon}\} = \begin{bmatrix} \varepsilon_S & \varepsilon_\theta \end{bmatrix}^T \tag{7}$$

$$\{\boldsymbol{\sigma}\} = [\boldsymbol{D}]\{\boldsymbol{\varepsilon}\} + \{\boldsymbol{\sigma_0}\} \tag{8}$$

In Eq.(7), ε_S is the Lagrangian strain along S, that is

$$\begin{aligned} \boldsymbol{\varepsilon_S} &= \frac{\partial X}{\partial S}\frac{\partial U}{\partial S} + \frac{\partial Y}{\partial S}\frac{\partial V}{\partial S} + \frac{\partial Z}{\partial S}\frac{\partial W}{\partial S} \\ &\quad + \frac{1}{2}\left[\left(\frac{\partial U}{\partial S}\right)^2 + \left(\frac{\partial V}{\partial S}\right)^2 + \left(\frac{\partial W}{\partial S}\right)^2\right] \\ &\doteqdot \frac{\partial X}{\partial S}\frac{\partial U}{\partial S} + \frac{\partial Y}{\partial S}\frac{\partial V}{\partial S} + \frac{\partial Z}{\partial S}\frac{\partial W}{\partial S} \end{aligned} \tag{9}$$

The torsional strain ε_θ in Eq.(7), on the other hand, is defined as

$$\varepsilon_\theta = \frac{\partial \theta}{\partial S} \tag{10}$$

Furthermore, the elasticity matrix $[\boldsymbol{D}]$ and the initial stress vector in Eq.(8) $\{\boldsymbol{\sigma_0}\}$ are given, respectively, by

$$[\boldsymbol{D}] = \frac{1}{A}\begin{bmatrix} AE & B_T \\ B_T & GJ \end{bmatrix} \tag{11}$$

$$\{\boldsymbol{\sigma_0}\} = \frac{1}{A}\begin{bmatrix} T \\ M_t \end{bmatrix} \tag{12}$$

where B_T is an axial-torsional coupling parameter[5].

The strain-displacement relationship matrix $[\boldsymbol{B}]$ considering the effect of geometric nonlinearity and the elastic stiffness matrix of the element, $[\boldsymbol{K}^e]$, now can be computed explicitly in the global coordinate system by using the following relation:

$$[\boldsymbol{K}^e] = \int_0^{L_c} A[\boldsymbol{B}]^T [\boldsymbol{D}][\boldsymbol{B}]\, dS \tag{13}$$

On the other hand, the geometric stiffness matrix of the element, $[\boldsymbol{K}_\sigma^e]$, can be derived in the global system as

$$[\boldsymbol{K}_\sigma^e] = \int_0^{L_c} [\boldsymbol{G}]^T \left[\tilde{\boldsymbol{S}}\right][\boldsymbol{G}]\, dS \tag{14}$$

The end-restraint springs in Fig. 1 are used for modeling the tensile restraints provided by a series of transmission towers located beyond either end of the system. In the current study, the stiffness of any end-restraint spring placed along certain direction will be chosen as 1.5 times the stiffness of a single tower, measured in the same direction as that of the spring.

2.2 Tower structures

The component members of each transmission tower in the system will be modeled by using 3-D beam-column elements. In taking the effect of geometric nonlinearity into account, a Cartesian coordinate system composed of x-, y- and z-axes as illustrated in Fig. 3 is adopted as the local coordinate system of the beam-column element. In undertaking the seismic time-history analysis, Newton-Raphson method will be adopted as the iterative scheme for modifying the stiffness coefficients repeatedly at each time step until the attainment of convergence.

2.3 Soil-structure interaction

Since the seismic responses of the transmission tower is closely related to the properties of the soil in the vicinity of the tower base, it would be essential to take the soil-structure interaction into consideration. According to the method of consistent infinitesimal finite-element cell [2-4], there exists a layer of finite-element cell between the borders of near-field and far-field soils. The interfaces at both interior and exterior boundaries of the finite-element cell are assumed geometrically similar with each other, and the thickness of the cell is assumed to be

$$h_c = r_e - r_i \tag{15}$$

Recognizing that h_c is the parameter with infinitesimal magnitude, one can derive the stiffness matrix of the cell, $[\boldsymbol{K}^*]$, by following the standard finite-element procedures without difficulty. Denoting the interaction force acting on near-field soil by using the symbol $\{\mathbf{Q}(t)\}$, one can then express the equations of motion for the system consisting of superstructure and near-field soil in the matrix form as

$$\begin{aligned} &[\mathbf{M}]\{\ddot{\mathbf{U}}(t)\} + [\mathbf{C}]\{\dot{\mathbf{U}}(t)\} + [\mathbf{K}]\{\mathbf{U}(t)\} = \\ &-[\mathbf{M}]\{\mathbf{I}\}\ddot{u}_g(t) + \{\mathbf{Q}(t)\} \end{aligned} \tag{16}$$

Denoting $\{\boldsymbol{R}(t)\}$ as the interaction force

acting on far-field soil leads to

$$\{\boldsymbol{Q}(t)\} = -\{\boldsymbol{R}(t)\} \tag{17}$$

The force-displacement relationship of the far-field soil can be written in the frequency domain as

$$\{\boldsymbol{R}(\omega)\} = \left[\boldsymbol{S}^{\infty}(\omega)\right]\{\boldsymbol{U}(\omega)\} \tag{18}$$

If $\left[\boldsymbol{S}^{\infty}(t)\right]$ is the inverse Fourier transform of $\left[\boldsymbol{S}^{\infty}(\omega)\right]$, then $\{\boldsymbol{R}(t)\}$ is given by

$$\{\boldsymbol{R}(t)\} = \int_0^t \left[\boldsymbol{S}^{\infty}(t-\tau)\right]\{\boldsymbol{U}(\tau)\}d\tau \tag{19}$$

The mass matrix $\left[\boldsymbol{M}^{\infty}(\omega)\right]$ corresponding to dynamic-stiffness matrix $\left[\boldsymbol{S}^{\infty}(\omega)\right]$ in frequency domain can be expressed as

$$\left\{\boldsymbol{M}^{\infty}(\omega)\right\} = \frac{\left[\boldsymbol{S}^{\infty}(\omega)\right]}{(i\omega)^2} \tag{20}$$

from which Eq.(19) is now able to be written in an alternate form:

$$\{\boldsymbol{R}(t)\} = \int_0^t \left[\boldsymbol{M}^{\infty}(t-\tau)\right]\left\{\ddot{\boldsymbol{U}}(\tau)\right\} d\tau \tag{21}$$

The force-displacement relationship of the finite-element cell located between the interior and exterior boundaries is written as

$$\left[\boldsymbol{S}(\omega)\right]\{\boldsymbol{U}(\omega)\} = \{\boldsymbol{P}(\omega)\} \tag{22}$$

Partitioning the degrees of freedom into those corresponding to interior and exterior boundaries separately yields

$$\begin{bmatrix} \left[\boldsymbol{S}_{ii}(\omega)\right] & \left[\boldsymbol{S}_{ie}(\omega)\right] \\ \left[\boldsymbol{S}_{ei}(\omega)\right] & \left[\boldsymbol{S}_{ee}(\omega)\right] \end{bmatrix} \begin{Bmatrix} \{\boldsymbol{U}_i(\omega)\} \\ \{\boldsymbol{U}_e(\omega)\} \end{Bmatrix} = \begin{Bmatrix} \{\boldsymbol{P}_i(\omega)\} \\ \{\boldsymbol{P}_e(\omega)\} \end{Bmatrix} \tag{23}$$

in which the subscripts *i* and *e* are used to denote the conditions associated with interior and exterior boundaries respectively. Evidently, the nodal forces of the finite-element cell and the interaction force acting on the far-field soil would be related to each other as expressed by

$$\{\boldsymbol{P}_i(\omega)\} = \{\boldsymbol{R}_i(\omega)\} \tag{24}$$

$$\{\boldsymbol{P}_e(\omega)\} = -\{\boldsymbol{R}_e(\omega)\} \tag{25}$$

in which $\{\boldsymbol{R}_i(\omega)\}$ and $\{\boldsymbol{R}_e(\omega)\}$ are given, respectively, as

$$\{\boldsymbol{R}_i(\omega)\} = \left[\boldsymbol{S}_i^{\infty}(\omega)\right]\{\boldsymbol{U}_i(\omega)\} \tag{26}$$

$$\{\boldsymbol{R}_e(\omega)\} = \left[\boldsymbol{S}_e^{\infty}(\omega)\right]\{\boldsymbol{U}_e(\omega)\} \tag{27}$$

Performing the algorithm of inverse Fourier transformation for obtaining the governing equations in time domain first, and then discretizing this domain afterward, one would obtain the acceleration unit-impulse response $\left[\boldsymbol{M}^{\infty}(t)\right]_{\boldsymbol{n}}$ $(\boldsymbol{n} = 1, 2, \cdots, \boldsymbol{N})$, corresponding to the nth time step. With the assumption of uniform variation in acceleration within each time interval Δt, Eq.(21) can be rewritten as

$$\{\boldsymbol{R}(t)\} = \left[\boldsymbol{M}'\right]\left\{\ddot{\boldsymbol{U}}(t)\right\} + \{\boldsymbol{F}'\} \tag{28}$$

Accordingly, the equations of motion in Eq.(16) can be expressed by

$$\begin{aligned} &\left(\left[\mathbf{M}\right] + \left[\mathbf{M}'\right]\right)\left\{\ddot{\mathbf{U}}(t)\right\} + \left[\mathbf{C}\right]\left\{\dot{\mathbf{U}}(t)\right\} + \left[\mathbf{K}\right]\{\mathbf{U}(t)\} \\ &= -\left[\mathbf{M}\right]\{\mathbf{I}\}\ddot{u}_g(t) - \{\mathbf{F}'(t)\} \end{aligned} \tag{29}$$

3. Failure index

It is recognized that the fracture of beam-column members is not purely caused by a single type of internal forces but by the combined action of several kinds of internal forces including axial, flexural, shear and perhaps torsional forces in usual. According to the investigation undertaken by Kitipornchai, Zhu, Xiang and Al-Bermani, the yield criterion of beam-column elements in angle sections behaving in an elastic-perfectly manner can be defined as [6]

$$\begin{aligned} \tilde{\Phi}(p, m_x, m_y) = &\frac{4}{27}\tilde{\lambda}^3(\tilde{\xi} - 1) \\ &+ (\tilde{\Omega} + \tilde{\mu})^3 \, sign(1, p) \\ &- 3(\tilde{\Omega} + \tilde{\mu})(\frac{\tilde{\phi}}{\tilde{\gamma}})^2 \, sign(1, p) \\ &+ \tilde{\lambda}(\tilde{\Omega} + \tilde{\mu})^2 + \tilde{\lambda}(\frac{\tilde{\phi}}{\tilde{\gamma}})^2 = 0 \end{aligned} \tag{30}$$

where

$$\tilde{\Omega} = 0.7071(m_x + \tilde{\alpha} m_y + \tilde{\beta}) \tag{31}$$

$$\tilde{\phi} = 0.7071(-m_x - \tilde{\alpha} m_y + \tilde{\beta}) \tag{32}$$

$$\begin{aligned} \tilde{\alpha} = &0.7279 + 0.1038|p| + 6.64667\,p^2 \\ &- 13.6904|p|^3 + 7.0038\,p^4 \\ &- 0.03586\sin(2\pi|p|) \\ &+ 0.1554\cos(2\pi p) \end{aligned} \tag{33}$$

$$\tilde{\beta} = -0.04262 - 0.4450|p| + 3.07857p^2 - 3.6351|p|^3 + 1.0002p^4 - 0.06855\sin(2\pi|p|) + 0.04262\cos(2\pi p) \quad (34)$$

$$\tilde{\gamma} = 1.61772 - 0.5039|p| + 2.8671p^2 - 2.6321|p|^3 - 0.00476p^4 + 0.06688\sin(2\pi|p|) + 0.05107\cos(2\pi p) \quad (35)$$

$$\tilde{\xi} = 1.5186 - 1.9165|p| - 16.3988p^2 + 42.0945|p|^3 - 23.8371p^4 + 0.3236\sin(2\pi|p|) - 0.5536\cos(2\pi p) \quad (36)$$

$$\tilde{\lambda} = 1.2 + 8.395(0.9 - |p|)^2 \quad (37)$$

$$\tilde{\mu} = -0.009195 + 0.3133|p| - 1.8183p^2 + 1.4675|p|^3 + 0.0455p^4 - 0.07293\sin(2\pi|p|) + 0.00919\cos(2\pi p) \quad (38)$$

In the above equations, the dimensionless parameters, p , m_y and m_z , are defined, respectively, as

$$p = \frac{P}{P_y} \;\; ; \;\; m_y = \frac{M_y}{M_{py}} \;\; ; \;\; m_z = \frac{M_z}{M_{pz}} \quad (39)$$

In deriving the Eq.(30), normality condition to the flow rule of plastic deformations have been employed and the shear influence on yielding is ignored.

Since the global failure of the transmission tower can be triggered by the fracture of any single main leg in the structure, the term "failure index" will be designated to the parameter Λ , which is assumed following the relation given by

$$\log \Lambda = \tilde{\Phi} \quad (40)$$

Accordingly, for the cases where the failure index, Λ , is smaller than 1, an elastic stress state exits, whereas when the index corresponding to any section of the beam-column element reaches to unity, the fracture of the member occurs.

4. Numerical examples and discussion

The acceleration records of Chi-Chi earthquake measured at TCU084 station in Taichung, Taiwan, having a peak value of $1.00834g$ and the Fourier spectrum as shown in Fig. 6 is taken as the ground excitation of the structural systems discussed in the following. As indicated in Fig.1, each of the structural systems investigated in the following will include three tower structures, among which the towers M and N are located on sides, and the tower O is located in the middle of the system. Fig. 7 shows the structural pattern for each tower in the system. Besides, to investigate the effect of soil-structure interaction, three kinds of soil, denoted as soil type I, soil type II and soil type III, having the values of modulus of elasticity 6×10^7 , 1.2×10^8 and 1.8×10^8 N/m^2 respectively, will be utilized. Each type of soil is assumed having a Poisson's ratio of 0.35 and a mass density of 1800 kg/m^3.

For simplification of calculations, the investigation regarding to the internal-force variation will be mainly focused upon the four leg-members denoted as Leg A, Leg B, Leg C and Leg D respectively and located at the lowest portion of tower N. The horizontal and vertical positions of tower N relative to towers M and O contained in the structural systems will be described by using the parameters θ and ϕ respectively. Figs. 8 and 9 illustrate the definitions of these two parameters.

4.1 Variation of Λ due to θ or ϕ

Two phenomena will be easily found by making observation of Fig. 10 to Fig. 13 as follows: (1) The peak values of Λ would usually occur at the moment when the seismic force acts in the direction parallel to the tower-base diagonals, which passes through Legs A and C at $\lambda = 45°$ and through Legs B and D at $\lambda = 135°$, respectively. (2) The larger the value of θ or ϕ is the larger Λ will usually be. In addition, it can be found by making the comparison between Figs. 10 and 13 that under any fixed value of λ, the failure index corresponding to the cases where the variation of line configurations occurs in horizontal plane only (referring to Fig. 10) would possess the values somewhat larger than those in the condition of $\phi \neq 0°$. This

implies that the extent of strength reduction for tower main-legs due to the variation of line configurations in horizontal plane only is usually more significant than that in vertical plane only.

4.2 Cable-mass participation in responses

The electrical wires connected with transmission towers and lining up in the air over a large span, although possessing pretty low rigidity, are expected making a significant contribution to the seismic responses of tower members due to the great increase in total system mass from the cables themselves. Figs. 14, 15 and 16 show the variation of Λ corresponding to the cases including all cable effects being excluded, cable-masses being excluded only and all cable effects being included, with respect to the tower systems under various line configurations respectively. It is shown in all figures that in comparison with the cable stiffness, the cable mass actually dominates the contribution to seismic responses of tower members. This is because the joining of cable-mass to the structural system leads to the shifting of the fundamental frequency from a value lower than the dominated frequency of the earthquake adopted (in the vicinity of 7.3 rad/sec as indicated in Fig. 6) to the one even much lower than before. As a consequence, one may agree that cable-mass participation in total responses would be one of the most important and intriguing themes in seismic analyses of transmission-tower systems.

4.3 Variation of Λ due to soil properties

Although it would be usually the most convenient and efficient way to solve soil-structure interaction problems in frequency domain, this strategy is, however, not allowed to be used in the cases where the effect of geometric nonlinearity is intended to be considered in component members of the structure. The reason is due to the fact that the iteration algorithm utilized in nonlinear analysis can only be implemented in time domain. The aforementioned method of consistent infinitesimal finite-element cell, since being derived through time domain, would be appropriate to be used in this study for investigating the effect of soil-structure interaction. Figs. 17, 18 and 19 show the variation of Λ corresponding to soil types I, II and III, under various line configurations respectively. It is observed that the stiffer the soil surrounding the base of the tower is the higher Λ will usually be. Moreover, to make a further investigation into the effect of soil properties upon structural behaviors, both the absolute displacements at the bottom of Leg C and the relative displacements between the top and the bottom of the same member corresponding to various types of soil are illustrated in Figs. 20, 21 and 22. Although larger displacements will usually be found at the bottom of the main leg in the cases associated with the softer soil, the values of Λ are, however, larger in the cases associated with the stiffer soil. In other words, the variation tendencies of Λ corresponding to various soil properties are similar to those of the relative displacement but not of the absolute displacement at the bottom of the member.

5. Conclusions

Having undertaken the seismic analysis in consideration of the effect of geometric nonlinearity, with respect to the structural system modeled by using efficient cable elements, beam-column elements, end-restraint elements and the infinitesimal finite-element cell associated with soil-structural interaction, one may learn that the ignorance of cable contribution to total seismic responses, especially the portion from the cable mass, would induce significant errors in predicting the ultimate strength of tower members.

The larger the value of θ or ϕ is the larger Λ will usually be. In the condition of either varied θ or ϕ, the peak value of failure index of any main leg-member would usually be found at the moment when the seismic force acts in the direction parallel to the tower-base diagonal passing through the leg member considered. Furthermore, it is found under any fixed value of input angle of seismic angle, the failure index corresponding to the cases of

$\phi = 0^\circ$ and $\theta \neq 0^\circ$ would possess the values somewhat larger than those in the condition of $\theta = 0^\circ$ and $\phi \neq 0^\circ$, that is the extent of strength reduction for tower main-legs due to θ is more significant than that to ϕ for the cases considered.

The stiffer the soil surrounding the base of the tower is the higher failure index in the main leg-member will usually be. Moreover, it is found in the leg member that the variation tendencies of failure index corresponding to various soil properties are similar to those of the relative displacement but not of the absolute displacement, at the bottom of the member, which is usually more significant under the softer soil.

References

1. Desai Y., Yu P., Popplewell N., Shah A., Finite Element Modeling of Transmission Line Galloping. Computers & Structures. 1995; 57(3): 407-420.
2. Wolf JP, Song C. Dynamic-Stiffness Matrix in Time Domain of Unbounded Medium by Infinitesimal Finite Element Cell Method. Earthquake Engineering and Structural Dynamics 1994; 23(11): 1181-1198.
3. Song C, Wolf JP. Consistent Infinitesimal Finite-Element-Cell Method: Three-Dimensional Vector Wave Equation. International Journal for Numerical Methods in Engineering 1996; 39: 2189-2208 .
4. Wolf JP, Song C. Finite-Element Modeling of Unbounded Media. New York: John Wiley & Sons Ltd, 1997.
5. Desai Y., Popplewell N., Shah A., Buragohain D., Geometric Nonlinear Static Analysis of Cable Supported Structures. Computers & Structures. 1988; 29(6): 1001-1009.
6. Kitipornchai S., Zhu K., Xiang, Y., AlBermani FGA, Single-equation Yield Surface for Mono-symmetric and Asymmetric Sections. Eng. Struct. 1991; 13(10): 366-370.

Fig 1. Analytical model of tower system

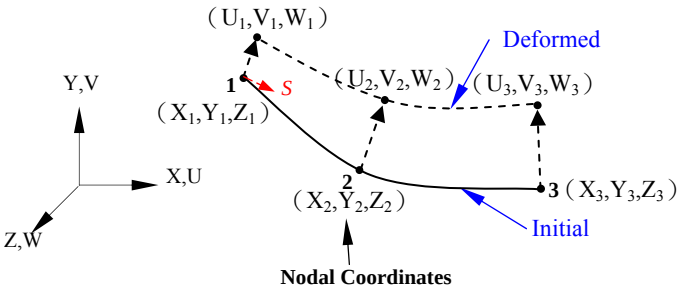

Fig 2. Deformed configuration for parabolic cable element

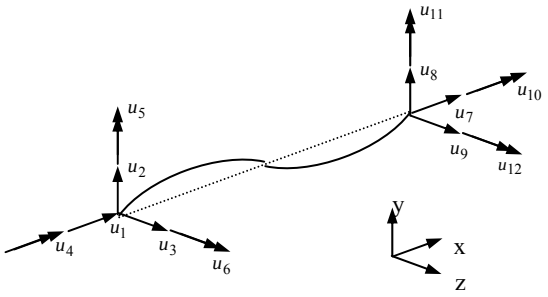

Fig 3. Nodal displacement of 3-D beam-column element

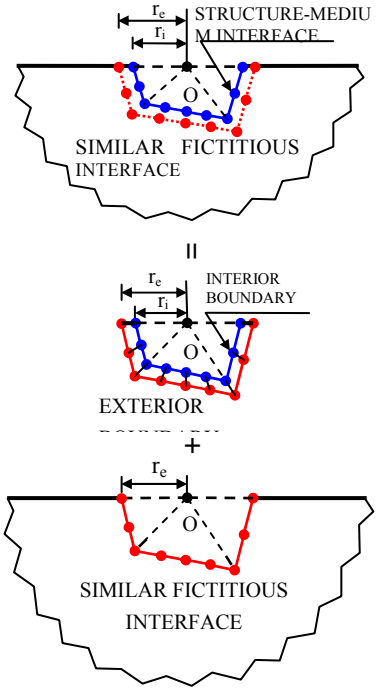

Fig 4. Infinitesimal finite-element cell and similar fictitious interface

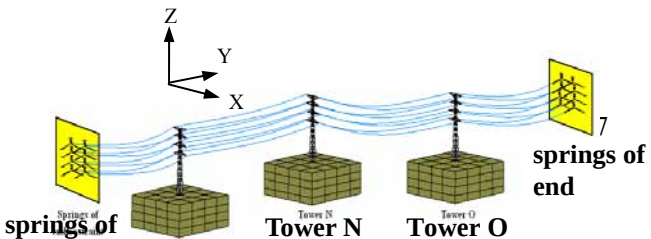

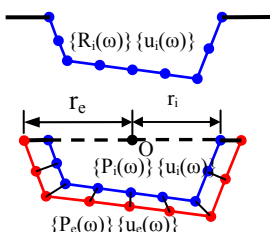

Fig 5. Nodal forces of finite-element cell and interaction forces at interior and exterior boundaries

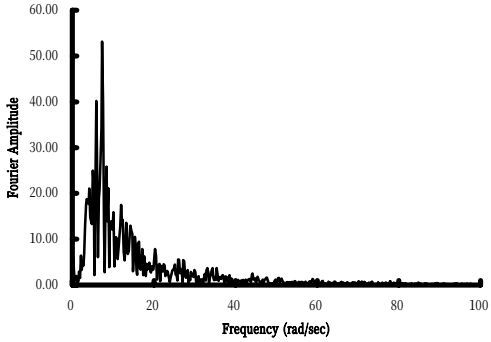

Fig 6. Fourier spectrum of earthquake acceleration

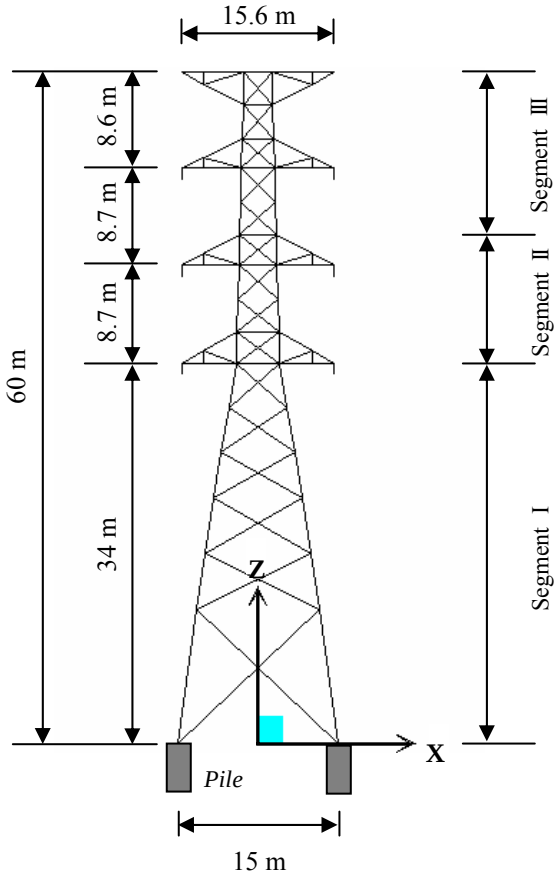

Fig 7. Structural pattern of transmission tower

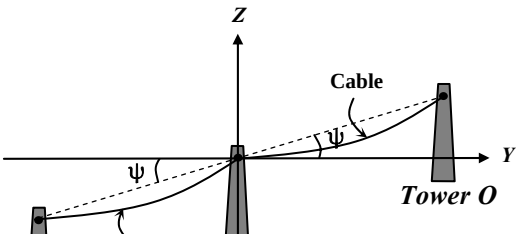

Fig 8. Description of horizontal line-angle θ

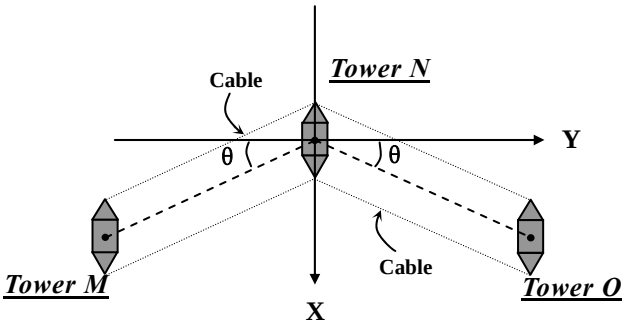

Fig 9. Description of vertical line-angle ψ

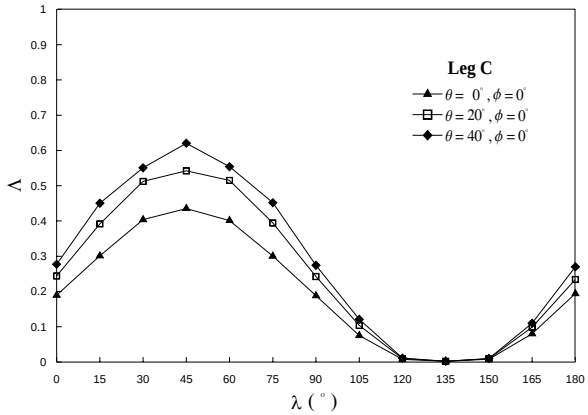

Fig 10. Failure index of Leg C with $\phi = 0^{\circ}$ under varied θ

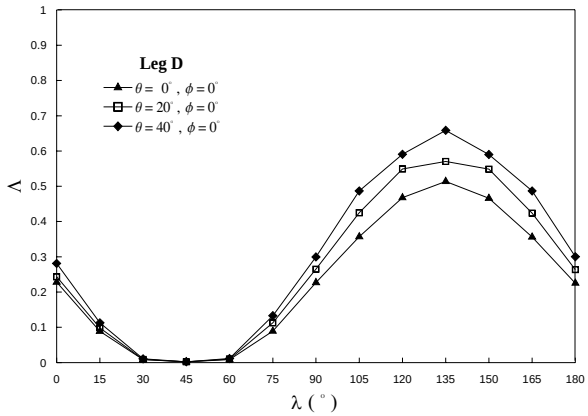

Fig 11. Failure index of Leg D with $\phi = 0^{\circ}$ under varied θ

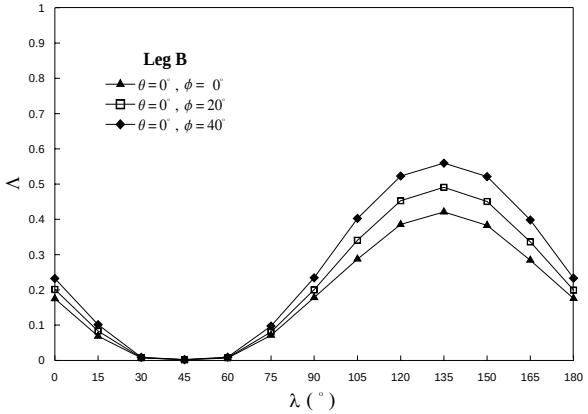

Fig 12. Failure index of Leg B with $\theta = 0^o$ under varied ϕ

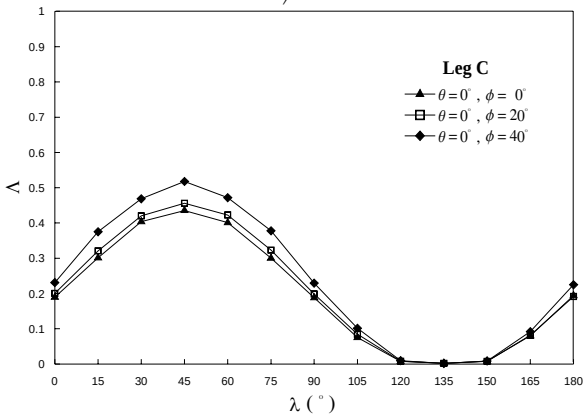

Fig 13. Failure index of Leg C with $\theta = 0^o$ under varied ϕ

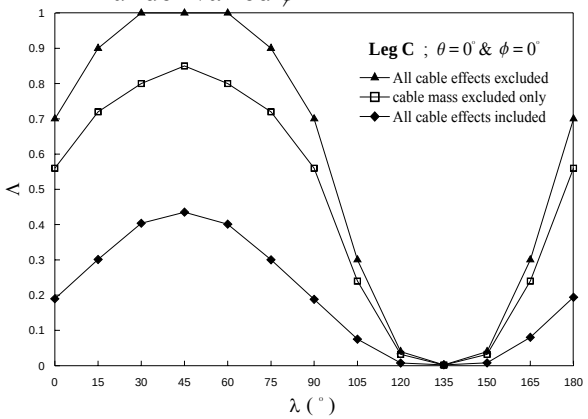

Fig 14. Failure index considering cable-mass effect with $\theta = \phi = 0^o$

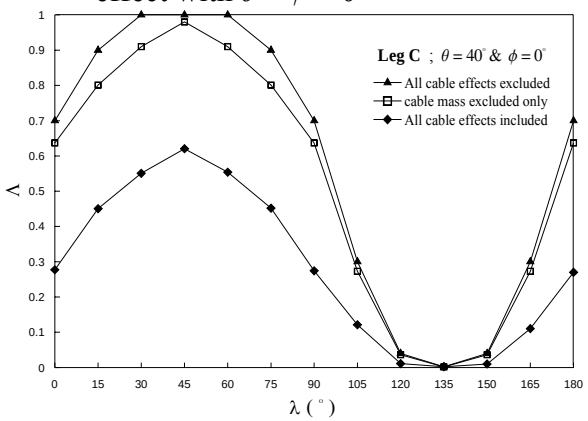

Fig 15. Failure index considering cable-mass effect with $\theta = 40^o$ & $\phi = 0^o$

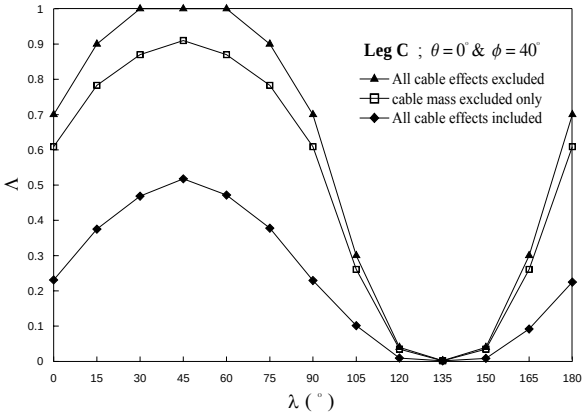

Fig 16. Failure index considering cable-mass effect with $\theta = 0^o$ & $\phi = 40^o$

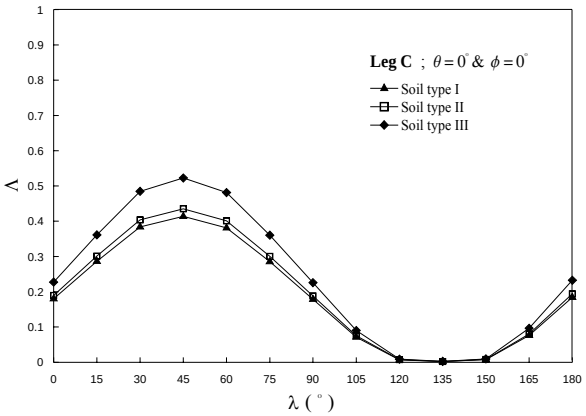

Fig 17. Failure index with $\theta = \phi = 0^o$ under various soil properties

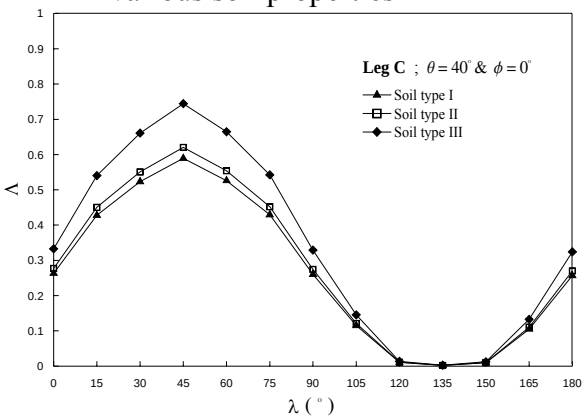

Fig 18. Failure index with $\theta = 40^o$ & $\phi = 0^o$ under various soil properties

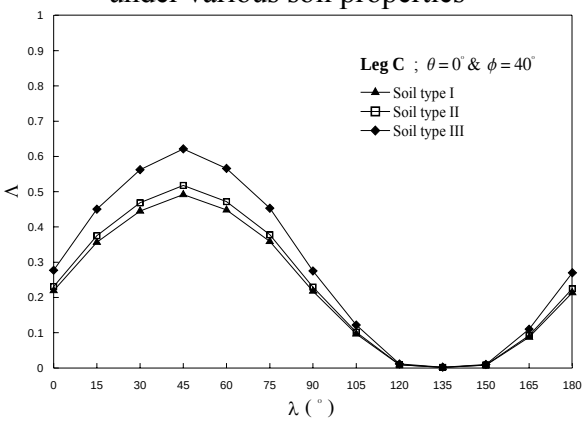

Fig 19. Failure index with $\theta = 0^o$ & $\phi = 40^o$ under various soil properties

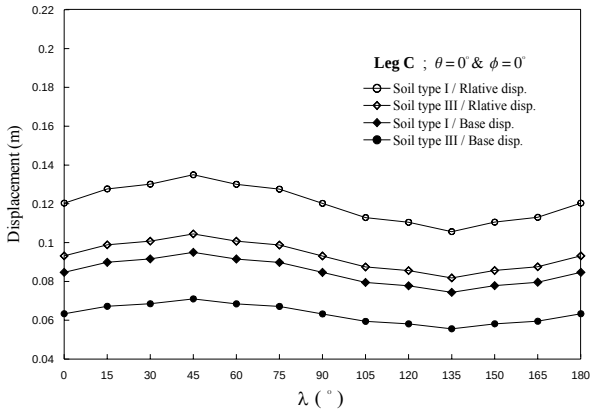

Fig 20. Base and relative disps. with $\theta = \phi = 0^{o}$ under various soil properties

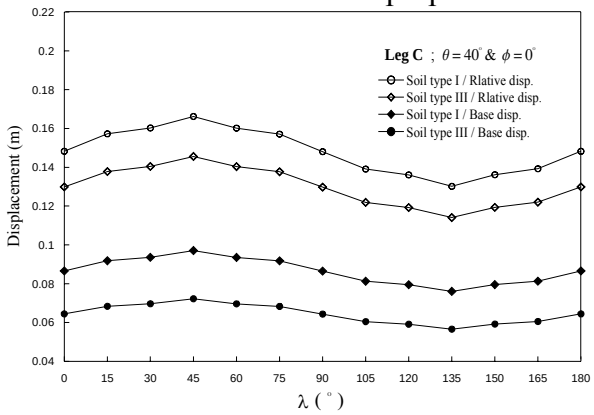

Fig 21. Base and relative disps. with $\theta = 40^{o}$ & $\phi = 0^{o}$ under various soil properties

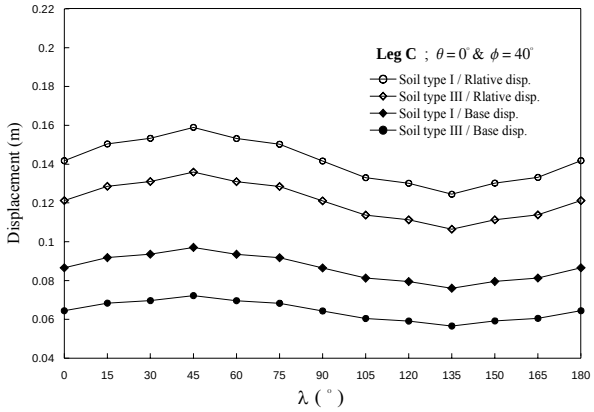

Fig 22. Base and relative disps. with $\theta = 0^{o}$ & $\phi = 40^{o}$ under various soil properties

Self-evaluation for the project

The themes discussed and the results obtained in this project are significant in both academic and practical aspects. It is expected that by aid of this project, structural engineers may gain a better insight into the roles played by the cable mass, soil properties and the configurations of transmission lines under strong earthquake.